Journal of Power Sources 248 (2014) 1021–1027

Contents lists available at ScienceDirect

Journal of Power Sources

journal homepage: www.elsevier.com/locate/jpowsour

Tyzor®-LA used as a precursor for the preparation of carbon coated TiO_2

Pier Paolo Prosini*, Cinzia Cento, Alfonso Pozio

ENEA, Italian National Agency for New Technologies, Energy and Sustainable Economic Development, Casaccia Research Centre, Via Anguillarese 301, Santa Maria di Galeria, Rome 00123, Italy

HIGHLIGHTS

- Carbon coated TiO_2 was prepared by decomposition of Tyzor®-LA.
- The TiO_2 was electrochemical characterized in lithium cell.
- The TiO_2 was used as an anode in lithium-ion battery.
- A severe capacity fade affected the battery when cycled at C/10.

ARTICLE INFO

Article history:
Received 3 July 2013
Received in revised form
3 October 2013
Accepted 7 October 2013
Available online 15 October 2013

Keywords:
Tyzor®-LA
Titanium oxide
Lithium iron phosphate
Lithium-ion battery

ABSTRACT

In this paper the preparation, the morphology, the structure and the electrochemical performance of carbon coated TiO_2 produced by using Tyzor®-LA as a precursor have been studied by using SEM, XRD and electrochemical methods. The electrochemical methods included low rate cycling, cycling at C-rate and cycling at different rates. At the same time the physical and electrochemical properties of $LiFePO_4$ were investigated by using the same methods. Lithium-ion batteries were prepared by sandwiching a glass fiber between a TiO_2 electrode used as the anode and a $LiFePO_4$ electrode used as the cathode and tested to evaluate cell performance.

1. Introduction

Lithium-ion batteries represent one of the most technologically advanced devices for energy storage, both for the high value of the achieved energy density and for the versatility of the product in terms of fast charge/discharge and good capacity retention. In terms of safety, lithium batteries suffer of an intrinsic instability mainly related to the negative electrode. The negative electrode of a lithium-ion battery is based on graphite or other carbonaceous materials able of reversibly intercalating lithium ions. The operating voltage of the negative electrode of a lithium-ion battery is very close to the potential for metallic lithium deposition. Battery overcharging or fast charging can determine the formation of metallic lithium on the negative electrode causing safety issues. In recent years, several works have been carried out to replace the carbonaceous materials used as anodes in lithium-ion batteries with other compounds characterized by a greater stability. Among them, TiO_2 is emerging as one of the most promising: it has a low and stable voltage plateau, low cost, high security, and long cycle life. However, low electrical conductivity, poor rate capability and poor cycling performance (caused by the structural changes occurring during the lithiation process) have limited its practical applications. Several efforts have already been attempted to address this problem by surface conductive coatings [1,2]. Thin carbon layers can reduce the aggregation and crystal growth of TiO_2 particles, and increase the electrical conductivity of anatase particles [3]. Carbon-stabilized anatase has been prepared directly by using anatase as a titanium source and organic precursors as a carbon source through decomposition of the precursors to form carbon [3–8]. Recently Tao et al. proposed a direct, one-step synthesis of C/anatase complex materials from mixtures of organic carbon and titanium solution [9]. In literature it is also possible to find several papers in which TiO_2 was used as an anode in lithium-ion batteries. Lee et al. used anodized TiO_2 nanotubes as an anode

* Corresponding author. Tel.: +39 06 3048 6978; fax: +39 06 3048 6357.
E-mail address: pierpaolo.prosini@enea.it (P.P. Prosini).

0378-7753/$ – see front matter © 2013 Elsevier B.V. All rights reserved.
http://dx.doi.org/10.1016/j.jpowsour.2013.10.020

for lithium-ion and lithium-air battery [10] and very recently Bi et al. [11] used amorphous TiO_2 nanotubes as an anode for rechargeable micro lithium-ion battery. To increase the energy density of the devices the TiO_2 based anodes are generally coupled with high potential cathode materials [12]. Nevertheless, also systems working at lower voltage, obtained by coupling titanium oxide anodes with low voltage cathode materials such as $LiFePO_4$, have been proposed [13]. This system can be useful for stationary applications where the energy density is of secondary importance with respect to other parameters such as system cost or safety. In order to further reduce the cost of the system, we tried to study a commercial product, called Tyzor®-LA [14], as a precursor for the preparation of electrochemical active TiO_2. The Tyzor®-LA is an organic titanate soluble in water and stable at pH around 7–8, manufactured by DuPont. It is used as a catalyst in applications such as esterification, transesterification, and condensation. The Tyzor®-LA is also used to promote the formation of cross-linked in polymerization reactions, as a promoter of the reaction of adhesion and for the formation of titanium dioxide on various polymeric substrates to increase the adhesion, the hardness of the surface, the reflection of light and heat, and the resistance to corrosion and scratch. In this work we demonstrated the possibility to use the Tyzor®-LA as a precursor to obtained carbon coated titanium oxide. The material was used to prepare composite electrodes. The electrodes were fully electrochemical characterized in lithium cells before to be coupled with a $LiFePO_4$ cathode to obtain a lithium-ion battery. And the battery was cycled at C/10 rate to evaluate its performance.

2. Experimental

Carbon coated TiO_2 was prepared by mixing the solution of Tyzor®-LA (DuPont) with Super P carbon. 0.1 g of carbon where dispersed in 3.23 g of Tyzor®-LA solution (containing about 13.6 wt.% of TiO_2). The mixture was put in a glass container and homogenized by exposure to ultrasonic waves for 60 min. After the ultrasonic treatment, the solvent was allowed to evaporate by heating the mixture in air at a rate of 0.5 °C min^{-1} up to 450 °C. The solid residue was kept at this temperature for 2.0 h. The solid was left to cool at room temperature. The final weight of the solid was 0.524 g, about 0.015 g less than the expected value. The weight lost is probably due to the carbon burned during the heating treatment. The amount of carbon in the sample calculated by thermogravimetric analysis was about 13% (data not shown). Crystalline $LiFePO_4$ was obtained by heating amorphous $LiFePO_4$ in a tubular furnace at 550 °C under a reducing atmosphere ($Ar/H_2 = 95/5$) for 1.0 h [15]. Amorphous $LiFePO_4$ was obtained by chemical lithiation of amorphous iron(III)phosphate using LiI as the reducing agent. Amorphous iron(III)phosphate was synthesized by spontaneous precipitation from an equimolar aqueous solution of $Fe(NH_4)_2(SO_4)_2 \cdot 6H_2O$ and $NH_4H_2PO_4$, using 30 wt.% hydrogen peroxide (Reagent grade, Ashland Chemical Italiana) as the oxidizing agent. Further experimental details can be found in Ref. [16]. The material morphology and composition were evaluated by a scanning electron microscope (SEM). High magnification microphotographs were obtained by using an AURIGA, CrossBeam Workstation dual column Focused Ion Beam – SEM equipped with an electron energy loss spectroscopy (EELS) system. The specimens were directly mounted onto a conductive carbon double face tape, which was previously mounted on a slab. The material structure was characterized by X-ray powder diffraction analysis (Rigaku Miniflex) using Cu-Kα radiation with a scan speed of 0.5 degrees per minute. For the electrode preparation, the $LiFePO_4$ and the carbon (Super P) with a ratio of 5:1 were mixed in a mortar for 5 min. The binder (Teflon, DuPont) was added and the blend was mixed to obtain a plastic-like material. The quantities of binder and carbon in the electrode were 8 wt.% and 17 wt.%, respectively. The percentage of active material in the cathode was 75 wt.%. No additional carbon was used to prepare the TiO_2 electrode. The TiO_2 powder, containing about 16.0% of carbon, was added with Teflon (8 wt.%) and mixed to obtain a plastic-like material. The active material in the anode was about 76%. Composite electrode tapes were made by roll milling the so obtained plastic-like materials. Electrodes were punched in the form of discs, typically with a diameter of 10 mm and a thickness of 90–100 μm. Polypropylene T-type pipe connectors with three cylindrical stainless steel (SS316) current collectors were used as electrochemical cells. To evaluate the electrode properties, lithium was used both as the anode and the reference electrode and a glass fiber was used as the separator. Lithium-ion battery cells were assembled by sandwiching a glass fiber between a TiO_2 anode and a $LiFePO_4$ cathode. A lithium disc orthogonally mounted with respect to the electrodes was used as the reference electrode. Lithium cells and lithium-ion batteries were filled with a 1 M solution of $LiPF_6$ in ethylene carbonate/diethyl carbonate (1/1). The cycling tests were automatically carried out with a battery cycler (Maccor 4000). Material handling, composite cathode preparation, cell assembly, test and storage were performed in a dry room (R.H. < 0.1% at 20 °C).

3. Results and discussion

3.1. Morphological and structural characterization

The Tyzor®-LA is a chelate of titanium and ammonium (Fig. 1). The main characteristics of the product are shown in Table 1. TiO_2 was obtained by heating at 450 °C for 2.0 h the solid material obtained after evaporation of the water. During the heating at high temperature the ammonium lactate was decomposed to form carbon dioxide and ammonia. The solid residue was analyzed by using XRD and SEM. Fig. 2 shows the results of the XRD analysis. Fig. 2 (left) shows the TiO_2 diffractogram. Although the intensity of the signal is very weak it is possible to observe the characteristic peaks belonging to the anatase phase. The peaks marked with an asterisk can be indexed as belonging to silicon oxide, that represents the main impurity. The silicon oxide can derive from the glass used to contain the solution during the ultrasonic treatment. Fig. 2 right shows the XRD pattern for the $LiFePO_4$ sample. The material shows the characteristic features of crystalline $LiFePO_4$ (card n° 40-1499) but the peaks are short and wide, indicating that the crystal structure has a short-range coherence.

Fig. 3 shows the SEM micrograph of the titanium oxide (left). The TiO_2 appear as a homogeneous material, with a flat surface on which it is possible to observe some protuberances probably formed by the gas evolved during the decomposition of the chelate. The EELS analysis (Table 2) shows that the samples is mainly

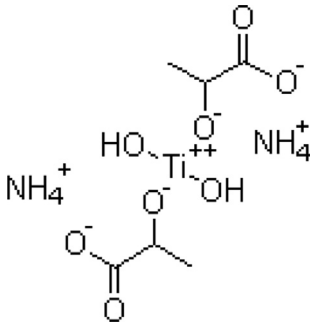

Fig. 1. Chemical formula of Tyzor®-LA.

Table 1
Chemical-physic characteristics of the Tyzor®-LA.

Tyzor®	% solvent	% TiO_2 content	Pour point, °C	Density, g cm^{-3}	Viscosity, MPa s	Flash point, °C
LA	50% Water	13.6	−10	1.21	N/A	None

formed by TiO_2 and contains silicon as the main impurity. The carbon is not uniformly dispersed in the sample at the microscopic level as assessed by the EELS analysis, and it was found to vary according to the area being analyzed. The minimum content of carbon found in the sample was 7.49 wt.% (Table 2). Several flakes of sub-micrometric dimensions are dispersed on the surface, and one of these can be observed on the bottom right of Fig. 3 left. The EELS analysis showed that these flakes have the same elemental composition of the bulk but are richer in carbon. Fig. 3 right shows a microphotograph of the lithium iron phosphate. It exhibits a very corrugated texture. The surface of the material appears formed by several globules of sub-micrometric dimensions, connected by a continue structure. The EELS analysis (Table 3) showed that the sample is rich in iron (the average phosphorus/iron atomic percentage was 0.82). The main impurities in the sample are carbon and sulfur, probably coming from the preparation method.

3.2. Electrochemical characterization of the electrodes

Fig. 4 shows the results of the electrochemical characterization of a TiO_2 electrode cycled between 1.4 and 2.5 V at C/10 rate. The active material load was 7.14 mg. On the left it is possible to observe the voltage profiles as a function of the electrode specific capacity (referred to the weight of the active material) while on the right the specific capacity and the charge coefficient (defined as the relationship between the amount of electricity that must be fed into the electrode to offset the previously discharged capacity) are reported. The first two discharge/charge voltage profiles differ from the profiles exhibited in the following cycles. The initial voltage of the electrode was 3.3 V. During the first discharge process the electrode voltage decreased and after 43 mAh g^{-1} it reached a plateau at 1.77 V. The voltage remained constant and after 157 mAh g^{-1} the voltage decreased with a constant slope reaching the end charge voltage. During the first charge process the voltage slowly reached a plateau at 1.87 V after 57 mAh g^{-1}. This voltage was kept constant until a capacity of 150 mAh g^{-1} was accumulated. After that the voltage started to increase to reach the end voltage condition. The specific capacity during the first cycle was 252 mAh g^{-1} in discharge and 195 mAh g^{-1} in charge. The material presented an irreversible first cycle capacity of about 22.5% of the initial discharged capacity. Considering that the slope at the end of the first discharge cycle is longer compared to others cycles and that the SEI formation on carbon surface starts around 1.8 V, it is possible to suppose that the observed irreversible capacity could be related to the decomposition of the solvent on carbon. The first cycle charge coefficient was as high as 1.30. Starting from the second cycle, the charge coefficient strongly decreased reaching a value very close to the unit. The value reached at the 3rd cycle was as low as 1.01 and it remained constant in following cycles. Fig. 5 (left) shows the voltage profiles as a function of the specific capacity for the $LiFePO_4$ electrode cycled at C/10 between 4.2 and 2.0 V. The active material load was 15.0 mg. On the right it is possible to observe the specific capacity and the charge coefficient. The initial voltage of the electrode was 3.25 V. Upon charge the electrode voltage increased to reach a plateau at 3.46 V. Upon discharge the voltage reached a plateau at 3.4 V and then suddenly reached the end discharge

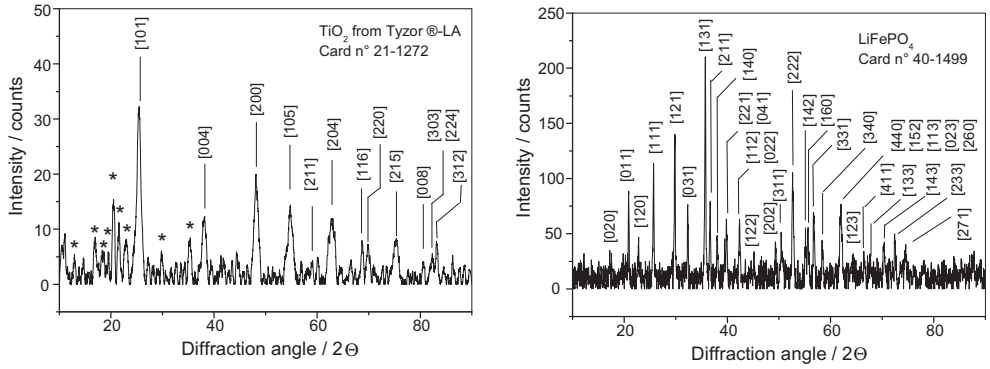

Fig. 2. XRD patterns of titanium oxide obtained starting from Tyzor®-LA (left) after annealing at 450 °C for 2.0 h in air and lithium iron phosphate (right) after annealing at 550 °C for 1.0 h under argon/hydrogen 95:5 atm.

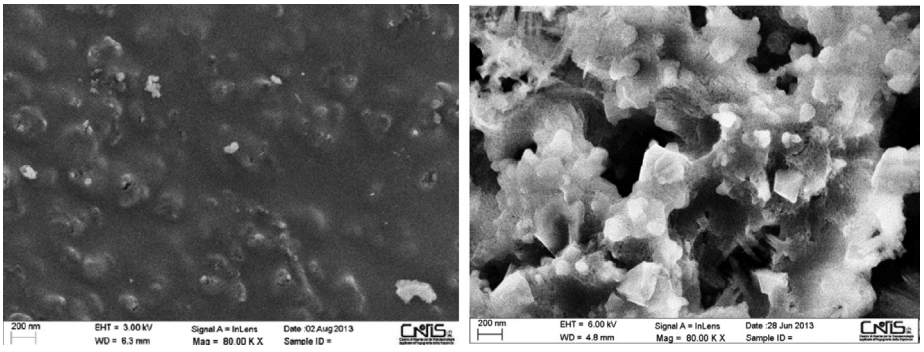

Fig. 3. Scanning electron micrographs of the titanium oxide obtained starting from Tyzor®-LA (left) and lithium iron phosphate (right).

Table 2
Electron energy loss spectroscopy of carbon coated TiO_2 after the heating treatment at 450 °C for 2.0 h.

Element	Wt.%	Atom.%	Error
Oxygen	41.04	59.98	6.41
Titanium	50.56	24.69	1.93
Carbon	7.49	14.58	1.51
Silicon	0.91	0.76	0.09

Table 3
Electron energy loss spectroscopy of $LiFePO_4$ after the heating treatment at 550 °C for 1.0 h.

Element	Wt.%	Atom.%	Error
Oxygen	48.98	70.26	6.66
Iron	32.05	13.17	1.97
Phosphorous	14.53	10.76	0.64
Carbon	2.20	4.21	0.75
Sulfur	2.23	1.60	0.14

voltage. The material was able to discharge 143 mAh g^{-1}, corresponding to about 0.84 Li equivalents. The voltage profiles in subsequent cycles were almost overlapped each other. The specific capacity during the first charge cycle was 137 mAh g^{-1} while it stabilized around 140 mAh g^{-1} in subsequent cycles (Fig. 5 right). The charge coefficient increased from 0.92 (value recorded at the first cycle) to 1.00 (recorded at the second cycle). The voltage profiles as a function of the specific capacity for the electrodes cycled at various discharge/charge rates are shown in Figs. 6 and 7. At the maximum charge rate (3C) the TiO_2 electrode was able to deliver 22 mAh g^{-1} (about 13% of the capacity delivered at C/10 rate) with an average charge voltage of 2.29 V. The effect of the current on the electrode performance is summarized in Fig. 6 right, where the specific capacity is plotted in a double logarithmic plot as a function of the specific current. The $LiFePO_4$ capacity was less sensitive to the current increase with respect to the TiO_2. For this reason it was possible to discharge the electrode at a maximum rate of 5C (Fig. 7 left). At this discharge rate, the electrode was able to deliver 59 mAh g^{-1} (about 42% of the capacity delivered at C/10 rate) at an average discharge voltage of 3.1 V. The effect of the current on the electrode performance is reported in Fig. 7 right, where the specific capacity is plotted in a double logarithmic plot as a function of the specific current. The capacity retention as a function of the cycle life is illustrated in Fig. 8 where the specific capacity is plotted as a function of cycle number for the cell containing the TiO_2 (left) and the $LiFePO_4$ (right). The cells were discharged at C-rate. Every 100 cycles a test cycle conducted at reduced current (C/10) was carried out to evaluate the specific capacity at a lower discharge rate. The capacity fade for the TiO_2 electrode after 800 cycles was 6.0% as evaluated during the reduced current test and 8.0% as evaluated during the C rate cycles. After the same number of cycles, the capacity retention for the $LiFePO_4$ electrode was higher: 0.3% as evaluated during the reduced current test and 2.1% as evaluated during the C rate cycles.

3.3. Electrochemical characterization of the lithium-ion battery

Fig. 9 (left) reports the voltage profiles for a lithium-ion battery prepared with $LiFePO_4$ as the cathode and TiO_2 as the anode cycled between 0.0 and 2.2 V for ten cycles. The $LiFePO_4$ active material

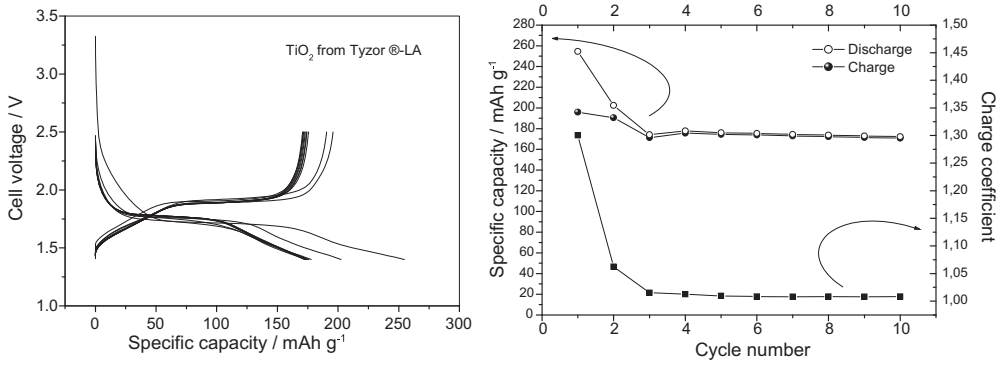

Fig. 4. Left: voltage profiles for a cell prepared with TiO_2 obtained starting from Tyzor®-LA and cycled at C/10 rate. Right: specific capacity in charge and discharge for the previous described cell. In the figure the charge coefficient (right axes) is also reported.

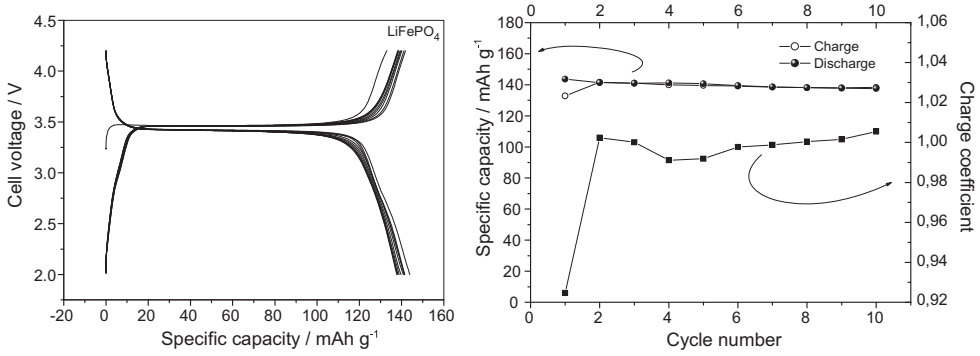

Fig. 5. Left: voltage profiles for a cell prepared with $LiFePO_4$ and cycled at C/10 rate (0.18 mA) for ten cycles. The active material load was 15 mg. Right: specific capacity in charge and discharge for the previous described cell. In the figure the charge coefficient (right axes) is also reported.

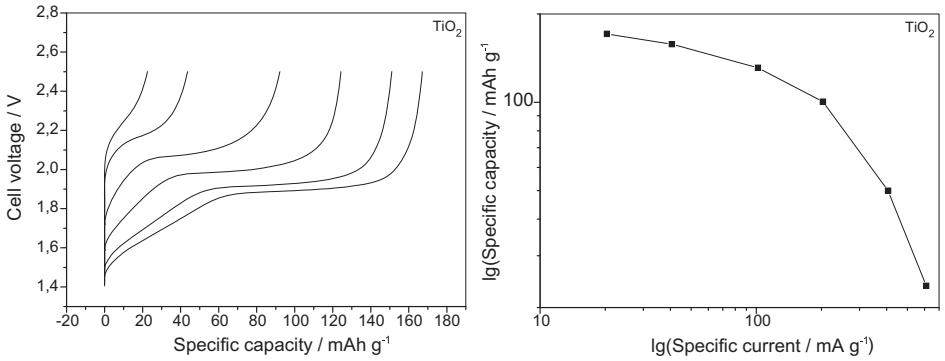

Fig. 6. Left: voltage profiles for the cell described in Fig. 4 cycled at various charge rates. The charge rates were C/10, C/5, C/2, 1C, 2C and 3C. Right: double logarithmic plot of the specific capacity as a function of the specific discharge current.

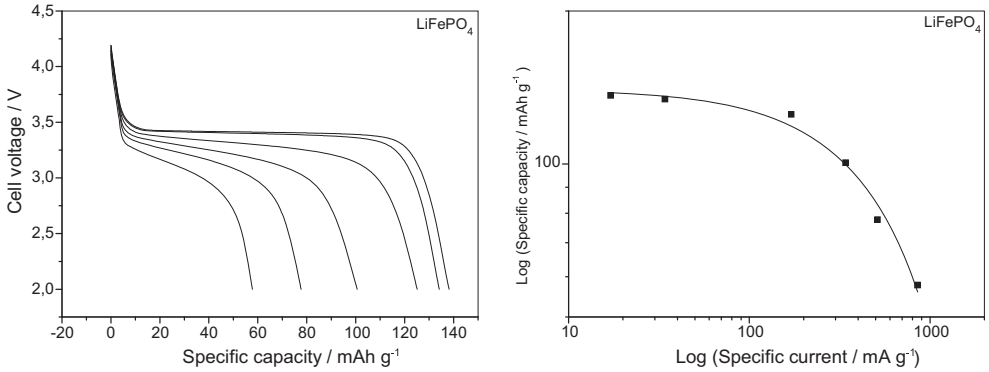

Fig. 7. Right: voltage profiles for the cell described in Fig. 5 cycled at various discharge rates. The discharge rates were C/10, C/5, C/1, 2C, 3C and 5C. Right: double logarithmic plot of the specific capacity as a function of the specific discharge current.

load was 14.0 mg. Considering the specific capacity of the $LiFePO_4$ evaluated during the first cycle at C/10 rate (137 mAh g^{-1}) the cathode capacity was about 1.92 mAh. The TiO_2 active material load was 7.2 mg. The specific capacity exhibited during the first discharge cycle was 252 mAh g^{-1}. By using this value the capacity of the anode was evaluated to be 1.81 mAh. From this calculation it results that the cell was anode limited and that the cathode capacity was about 5% higher than the anode capacity. The battery was cycled at 0.18 mA (C/10 rate). Two end charge conditions (ECC) were used. The first ECC was set with respect to the TiO_2 anode. The charge was stopped when the TiO_2 electrode voltage was lower than 1.4 V vs. Li. The second ECC was set with respect to the battery voltage that was limited to 2.2 V. The end discharge condition (EDC) was evaluated with respect to the battery voltage and set to 0.0 V. The initial voltage of the battery was about 0.0 V since both the electrodes in their initial state showed a similar voltage. After a charge of 55 mAh g^{-1} was passed into the cell (referred to the TiO_2 electrode), the voltage increased reaching a voltage plateau at 1.70 V. This plateau was kept constant until a charge of 150 mAh g^{-1} (referred to the TiO_2 electrode). After that the cell voltage increased reaching the first ECC. The total amount of current passed in this step was 1.84 mAh (about 255 mAh g^{-1} referred to the TiO_2 electrode), a little bit higher than the calculated anode capacity. Upon discharge the cell voltage decreased reaching a voltage plateau of 1.55 V. The voltage remained constant during the discharge process and it suddenly dropped off just before the EDC. The overall

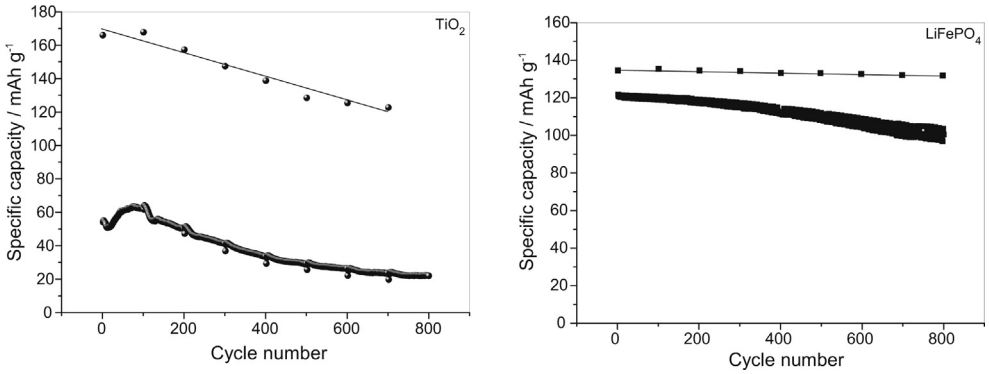

Fig. 8. Specific capacity as a function of the cycle number for a cell containing the TiO_2 (left) and the $LiFePO_4$ (right) cycled at C rate. A cycle at reduced current (C/10) was performed every 100 cycles to evaluate the specific capacity at a lower discharge rate.

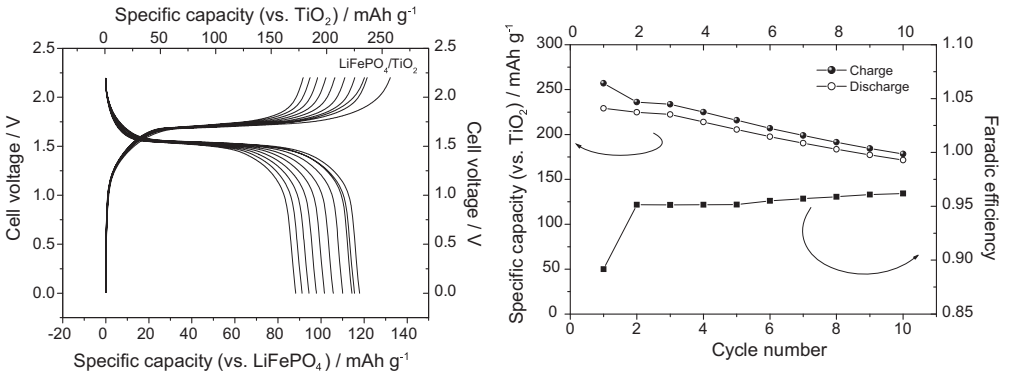

Fig. 9. Left: voltage profiles for a cell prepared with $LiFePO_4$ as a cathode and TiO_2 as an anode cycled at C/10 rate for ten cycles. Right: specific capacity in charge and discharge for the previous described cell. The specific capacity was referred to the sum of the weights of the active materials contained in both the electrode. In the figure the faradic efficiency (right axes) is also reported.

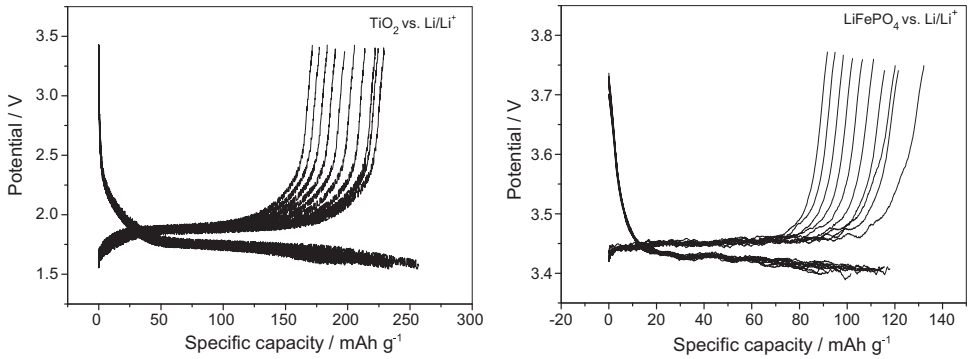

Fig. 10. Voltage profiles for the lithium-ion cell described in Fig. 9 referred to the TiO_2 electrode (left) and the $LiFePO_4$ electrode (right) recorded versus lithium metal used as the reference electrode.

discharged capacity was 1.65 mAh (about 225 mAh g^{-1} referred to the TiO_2 electrode). In the following cycles, the capacity in charge was always higher than the discharged one and a capacity fading affected the cell. In Fig. 9 right it is possible to observe the delivered specific capacity in charge and discharge (referred to the TiO_2 electrode), and the faradic efficiency (defined as the relationship between the amount of electricity restored and the amount of electricity fed into the cell). The cell presented a first cycle irreversible capacity of about 10.3% of the initial charged capacity. The first cycle faradic efficiency was 0.89. Starting from the second cycle, the faradic efficiency increased reaching a value of 0.96 after 10 cycles. The cell presented a severe capacity fading of about 2.5% per cycle. In Fig. 10 the voltage profiles of the TiO_2 (on the left) and the $LiFePO_4$ (on the right) electrodes for the previously described lithium-ion cell are reported with respect to lithium metal, used as the reference electrode. During the charge cycles the TiO_2 electrode never reached the first EDC (1.4 V vs. Li) while the voltage of the $LiFePO_4$ electrode was always higher than 3.7 V. Consequently the cell voltage reached the second ECC (2.2 V) without the TiO_2 was completely reduced. The end voltage of both the electrodes progressively increased by increasing the cycle number and at the 10th cycle the $LiFePO_4$ electrode and the TiO_2 electrode reached a voltage of 3.77 V and 1.52 V, respectively. From these evidences it follows that the cell was not anode limited. This result can be attributed to a lower capacity delivered by the cathode with respect the expected value. The low capacity of the cathode can be related to irreversible lithium-ion depletion during the first charge/discharge process probably due to the fact that a fraction of the lithium-ions inserted was trapped into the anode. As a consequence only a part of the Li-ions inserted in the TiO_2 during the charge step was removed in the subsequent cycle and reinserted into the $LiFePO_4$ determining an increase of the voltage of the positive electrode. The same effect (the trapping of lithium ion inside the negative electrode) can be evoked as responsible for the low value of the faradic efficiency and, consequently, for the capacity fade exhibited during the first ten charge/discharge cycles. To improve the battery performance further studies are needed, including a better choice of the charge procedure and an appropriate balancing of the electrode load.

4. Conclusions

In this paper the preparation and the electrochemical characterization of carbon coated TiO_2 produced from Tyzor®-LA was described. The material heated at 450 °C for 2.0 h showed the characteristic peaks belonging to the anatase phase. The electrochemical characterization in lithium cells allowed determining the specific capacity of the TiO_2 and its behavior as a function of current density and cycle number. The materials showed satisfactory capacity retention: it was able to cycle for over 800 times with a minimum capacity loss. Also the capacity retention as a function of the discharge current was satisfactory. The material was used as an anode in lithium-ion battery. $LiFePO_4$ with a low range order olivine structure were used as the cathode active material. Despite the electrochemical performance exhibited by the electrodes was very good, the lithium-ion battery, obtained by coupling the two electrodes, showed a high capacity fade upon cycling. The fade was related to the trapping of part of the lithium ions inside the negative electrode. A wrong balancing of the battery can explain the results reported in this paper. Better results might be obtained with

an appropriate balancing. To summarize, TiO_2 coming from Tyzor®-LA showed good electrochemical performances as an electrode in lithium cell but additional investigations are required to balance the load factor of the TiO_2 electrode and to improve the faradic efficiency in lithium-ion battery.

Acknowledgments

Part of this work was carried out within the activities "Ricerca Sistema Elettrico" funded through contributions to research and development by the Italian Ministry of Economic Development. We would thank the CNIS (Centro di ricerca per le Nanotecnologie applicate all'Ingegneria della Sapienza) for the implementation of SEM images.

References

[1] S. Yoon, B.H. Ka, C. Lee, M. Park, S.M. Oh, Electrochem. Solid State Lett. 12 (2009) A28–A32.
[2] M. Pfanzelt, P. Kubiak, U. Hörmann, U. Kaiser, M. Wohlfahrt-Mehrens, Ionics 15 (2009) 657–663.
[3] S.J. Park, Y.J. Kim, H.J. Lee, J. Power Sources 196 (2011) 5133–5137.
[4] M. Inagaki, F. Kojin, B. Tryba, M. Toyoda, Carbon 43 (2005) 1652–1659.
[5] T. Matsunaga, M. Inagaki, Appl. Catal. B 64 (2006) 9–12.
[6] B. Tryba, A.W. Morawski, T. Tsumura, M. Toyoda, M. Inagaki, J. Photochem. Photobiol. A 167 (2004) 127–135.
[7] P.Y. Chang, C.H. Huang, R.Y. Doong, Carbon 50 (2012) 4259–4268.
[8] J.S. Chen, H. Liu, S.Z. Qiao, X.W. Lou, J. Mater. Chem. 21 (2011) 5687–5692.
[9] Y. Tao, D. Yi, B. Zhu, J. Electron. Mater. 42 (2013) 783–786.
[10] B.G. Lee, S.-C. Nam, J. Choi, Curr. Appl. Phys. 12 (2012) 1580–1585.
[11] Z. Bi, M.P. Paranthaman, P.A. Menchhofer, R.R. Dehoff, C.A. Bridges, M. Chi, B. Guo, X.-G. Sun, S. Dai, J. Power Sources 222 (2013) 461–466.
[12] P.P. Prosini, R. Mancini, L. Petrucci, V. Contini, P. Villano, Solid State Ionics 144 (2001) 185–192.
[13] J. Hassoun, M. Pfanzelt, P. Kubiak, M. Wohlfahrt-Mehrens, B. Scrosati, J. Power Sources 217 (2012) 459–463.
[14] http://www2.dupont.com/Tyzor/es_MX/assets/downloads/K16498_tyzor_tech_info_final.pdf.
[15] P.P. Prosini, M. Carewska, S. Scaccia, P. Wisniewski, S. Passerini, M. Pasquali, J. Electrochem. Soc. 149 (2002) A886–A890.
[16] P.P. Prosini, M. Lisi, S. Scaccia, M. Carewska, F. Cardellini, M. Pasquali, J. Electrochem. Soc. 149 (2002) A297–A301.